Numerical Heat Transfer, Part B, 51: 67–96, 2007

ISSN: 1040-7790 print/1521-0626 online
DOI: 10.1080/10407790600710168

Taylor & Francis
Taylor & Francis Group

ON AN EQUAL FOURTH-ORDER-ACCURATE TEMPORAL/SPATIAL SCHEME FOR THE CONVECTION-DIFFUSION EQUATION

Tony W. H. Sheu and R. K. Lin
Department of Engineering Science and Ocean Engineering, National Taiwan University, Taipei, Taiwan, Republic of China

In this article, the convection-diffusion equation is discretized using the Pade method for the temporal derivative term and the wavenumber-extended method for the spatial derivative term. These temporal and spatial approximations result in two explicit equations and two implicitly coupled equations. To construct an equal-order scheme for the solution obtained at $n\Delta t$, both temporal/spatial derivatives are approximated to render fourth-order accuracy without using solutions obtained previously at $(n-2)\Delta t$, $(n-3)\Delta t$, etc. When approximating the first-order derivative term, it is essential to take the upwind nodal points into consideration. For revealing the dispersion and dissipation natures of the proposed scheme, both von Neumann (Fourier) and dispersion analyses were conducted. We validate the proposed method by solving several problems that are amenable to exact solutions. Results with theoretical rates of convergence are obtained for each of the one- and two-dimensional problems investigated.

1. INTRODUCTION

This article uses the finite-difference method to solve the practically and academically important one- and two-dimensional time-dependent convection-diffusion equation. A comprehensive survey of finite-difference methods and the available software packages to solve this class of differential equations have been provided by Shokin [1] and by Machura and Sweet [2], respectively. Method of lines (MOL) had been demonstrated to be effective for the integration of time-dependent parabolic [3], parabolic-elliptic [4], and Korteweg-de Vries [5] partial differential equations in fixed or adaptive grids. Within the MOL framework, the currently investigated parabolic equation is analyzed in two separate steps. First, the spatial derivatives are approximated by finite-difference/element/volume methods. This is followed by integrating the resulting system of semidiscrete equations. Existing techniques for solving the ordinary differential equation can thus be used to obtain the semidiscrete solution for the original partial differential equation. The simulated

Received 19 August 2005; accepted 4 March 2006.
Financial support provided by the National Science Council under Grant NSC 93-2611-E-002-002 is gratefully acknowledged.
Address correspondence to Tony W. H. Sheu, Department of Engineering Science and Ocean Engineering, National Taiwan University, No. 1, Sec. 4, Roosevelt Road, Taipei, 106 Taiwan, Republic of China. E-mail: twhsheu@ntu.edu.tw

NOMENCLATURE

C_g	group velocity	k_r	amplitude error defined in Eq. (4.7)
f	boundary force per unit volume	Pe	Peclet number
F	sufficiently differentiable function	R	reaction number
$\|G\|$	amplification factor	$\beta\,(\equiv k_m h)$	modified wavenumber
h	grid size	θ	phase angle
k_i	phase error defined in Eq. (4.8)	ν	Courant number
k_m	wavenumber defined in Eq. (4.3)	τ	$[\equiv \Delta t(\partial/\partial t)]$ defined in Eq. (2.4)

spatial and temporal error distributions have been studied extensively by Berzins [3, 6] and by Lawson et al. [4] and give an overall error at any MOL integration stage. One can refer to the book by Schiesser [7] for additional details about MOL methods. Since 1980, many software packages have been developed within the method-of-lines framework to solve the one-dimensional first-order time-dependent partial differential equations [8]. The software package SPRINT, which is included in the NAG Fortran library [9, 10], is a general-purpose software package, and new methods for spatial discretization, time integration, and matrix solvers can be integrated into its modular structure.

Among the available numerical methods to slove the initial-value equation, Euler's method is known to be one of the simplest ordinary differential equation solvers [11]. Since this method is numerically inefficient, the development of Taylor's method, which is time-consuming in calculating ϕ in $d\phi/dt = f$ but conceptually easy to manipulate, is therefore motivated. The need to overcome this drawback of Taylor's method prompted the development of one-step Runge-Kutta (RK) methods. Note that the Euler approach can be interpreted as a single-stage explicit RK scheme. There are many second-order two-stage and third-order three-stage explicit RK schemes in the literature [12]. The RK method of order $\bar{p}$ will generally introduce a local truncation error $O(h^{\bar{p}+1})$, provided that f is sufficiently differentiable [11]. Notice, however, that the use of higher-order RK methods requires more computational effort, which is the price paid for the improved accuracy.

To obtain high temporal accuracy in the approximation of ordinary differential equations, it is common practice to develop multistep methods to approximate the solution at the current time level [13]. The open-type fourth-order Adams-Bashforth (AB) method and the Adams-Moulton (AM) method [14–16] are used in the present article to assess the chosen time-stepping methods for the sake of comparison. Among the RK methods, the fourth-order four-stage explicit Runge-Kutta method has been widely used and is also considered as a benchmark method in the assessment of temporal schemes.

A reliable transport scheme must have the ability to suppress the convective instability [17–19]. One rational way to develop a convectively stable scheme is to take the analytic information of the investigated transport equation into consideration [20]. For the time derivative term, Pade's approximation [21–23] is employed to obtain temporal fourth-order accuracy. The resulting spatial equation, which takes inhomogeneous convection-diffusion-reaction (CDR) form, is discretized to yield the fourth-order spatial accuracy.

The rest of this article is organized as follows. Section 2 presents the working equation and the four-step Pade time-stepping scheme employed. This is followed by transformation of the time-dependent convection-diffusion equation into its equivalent steady-state convection-diffusion-reaction equation. In Section 3 the CDR finite-difference scheme employed to approximate the spatial derivative terms is proposed. Theoretical studies of the proposed scheme are conducted in Section 4 with emphasis on the dispersion and Fourier (or von Neumann) stability analyses. Section 5 presents simulated results to validate the method for both one-and two-dimensional problems. In Section 6, concluding remarks are given.

2. FOURTH-ORDER TEMPORAL DISCRETIZATION SCHEME

The following transport equation for ϕ is considered in this article:

$$\phi_t + u\phi_x + v\phi_y - k\nabla^2\phi = 0 \tag{2.1}$$

where k is the diffusion coefficient. Two variables u and v are denoted as the x- and y-direction velocities, respectively. Consider the following sufficiently differentiable function:

$$F = k\nabla^2\phi - (u\phi_x + v\phi_y) \tag{2.2}$$

Equation (2.1) can be rewritten as

$$\phi_t = F(\phi) \tag{2.3}$$

Unlike the method of lines, at first the approximation sequence can be reversed by approximating the time derivative term. Expansion of ϕ^{n+1} in a Taylor series with respect to ϕ at $t = n\,\Delta t$ yields

$$\phi^{n+1} = \left[1 + \Delta t\frac{\partial}{\partial t} + \frac{(\Delta t)^2}{2!}\frac{\partial^2}{\partial t^2} + \frac{(\Delta t)^3}{3!}\frac{\partial^3}{\partial t^3} + \cdots\right]\phi^n$$

By employing the relation given by $\exp(\tau) = 1 + \tau + 1/2!\ \tau^2 + 1/3!\ \tau^3 + \cdots$, ϕ^{n+1} can be expressed as

$$\phi^{n+1} = \exp(\tau)\phi^n \tag{2.4}$$

where $\tau = \Delta t\ \partial/\partial t$. We then apply the fourth-order-accurate Pade approximation [24] for $\exp(\tau)$ to yield

$$\exp(\tau) = \frac{1 + \frac{1}{2}\tau + \frac{1}{12}\tau^2}{1 - \frac{1}{2}\tau + \frac{1}{12}\tau^2} \tag{2.5}$$

Substitution of Eq. (2.5) into Eq. (2.4) allows us to derive

$$\left[1 - \frac{\tau}{2}\left(1 - \frac{1}{6}\tau\right)\right]\phi^{n+1} = \left[1 + \frac{\tau}{2}\left(1 + \frac{1}{6}\tau\right)\right]\phi^n \tag{2.6}$$

By virtue of the definitions for $\phi^{n+1/6} = (1 + \tau/6)\phi^n$ and $\tau = \Delta t(\partial/\partial t)$, the following equation can be derived:

$$\phi^{n+1/6} = \phi^n + \frac{\Delta t}{6}\phi_t^n \tag{2.7}$$

The scheme development is then followed by employing $\phi^{n+1/2} = \phi^n + (\tau/2)\phi^{n+1/6}$ and $\phi^{n+5/6} = [1 - (\tau/6)]\phi^{n+1}$ to derive

$$\phi^{n+1/2} = \phi^n + \frac{\Delta t}{2}\phi_t^{n+1/6} \tag{2.8}$$

and

$$\phi^{n+5/6} = \phi^{n+1} - \frac{\Delta t}{6}\phi_t^{n+1} \tag{2.9}$$

Use of Eqs. (2.6)–(2.8) enables us to obtain

$$\left[1 - \frac{\tau}{2}\left(1 - \frac{\tau}{6}\right)\right]\phi^{n+1} = \phi^{n+1/2} \tag{2.10}$$

By virtue of Eq. (2.9), the above equation can be rewritten as

$$\phi^{n+1} - \frac{\Delta t}{2}\phi_t^{n+5/6} = \phi^{n+1/2} \tag{2.11}$$

The Pade approximation employed for the temporal derivative term shown in Eq. (2.1) involves two implicit and two explicit equations for ϕ, as shown in Eqs. (2.12)–(2.13) and (2.14)–(2.15), respectively:

$$\phi^{n+1/6} = \phi^n + \frac{\Delta t}{6}F^n \tag{2.12}$$

$$\phi^{n+1/2} = \phi^n + \frac{\Delta t}{2}F^{n+1/6} \tag{2.13}$$

$$\frac{\Delta t}{6}F^{n+1} - \phi^{n+1} = -\phi^{n+5/6} \tag{2.14}$$

$$\frac{\Delta t}{2}F^{n+5/6} - \phi^{n+1} = -\phi^{n+1/2} \tag{2.15}$$

A description of our proposed calculation steps is given below.

(A) Calculate $\phi^{n+1/6}$ according to Eqs. (2.2) and (2.12):

$$\phi^{n+1/6} = \phi^n + \frac{\Delta t}{6}(-u\phi_x^n - v\phi_y^n + k\nabla^2\phi^n) \tag{2.16}$$

(B) Calculate $\phi^{n+1/2}$ according to Eqs. (2.2), (2.13), and (2.16):

$$\phi^{n+1/2} = \phi^n + \frac{\Delta t}{2}(-u\phi_x^{n+1/6} - v\phi_y^{n+1/6} + k\nabla^2\phi^{n+1/6}) \tag{2.17}$$

(C) Calculate ϕ^{n+1} according to

$$\phi^{n+1} = \phi^n + \Delta t(-u\phi_x^n - v\phi_y^n + k\nabla^2\phi^n) \tag{2.18}$$

(D) Calculate $\phi^{n+5/6}$ implicitly from Eq. (2.15) using the updated values of $\phi^{n+1/2}$ and ϕ^{n+1}:

$$\frac{\Delta t}{2}\left(u\phi_x^{n+5/6} + v\phi_y^{n+5/6} - k\nabla^2\phi^{n+5/6}\right) = \phi^{n+1/2} - \phi^{n+1} \tag{2.19}$$

(E) ϕ^{n+1} is then calculated implicitly from

$$\phi^{n+1} - \frac{\Delta t}{6}(-u\phi_x^{n+1} - v\phi_y^{n+1} + k\nabla^2\phi^{n+1}) = \phi^{n+5/6} \tag{2.20}$$

(F) Substitute ϕ^{n+1} into Eq. (2.19) to obtain $\phi^{n+5/6}$. Then substitute $\phi^{n+5/6}$ into Eq. (2.20) to obtain ϕ^{n+1}. The above procedures should be repeated until the L_2-norm of the computed difference between the consecutive iterations is less than the user's specified tolerance (10^{-13} is chosen in this study).

For the purpose of assessing the proposed fourth-order Pade scheme, the following fourth-order-accurate closed-type Adams-Moulton [16] and Gear two-step methods are considered:
Adams-Moulton method:

$$\phi^* = \phi^n + \frac{\Delta t}{24}(55F^n - 59F^{n-1} + 37F^{n-2} - 9F^{n-3}) \tag{2.21}$$

$$\phi^{n+1} = \phi^n + \frac{\Delta t}{24}(9F^* + 19F^n - 5F^{n-1} + F^{n-2}) \tag{2.22}$$

Gear method:

$$\phi^* = \frac{1}{3}(-10\phi^n + 18\phi^{n-1} - 6\phi^{n-2} + \phi^{n-3}) + 4\Delta t\ F^n \tag{2.23}$$

$$\phi^{n+1} = \frac{1}{25}(48\phi^n - 36\phi^{n-1} + 16\phi^{n-2} - 3\phi^{n-3}) + \frac{12}{25}\Delta t F^* \tag{2.24}$$

where $F^* = F(t^{n+1}, \phi^*)$. For the sake of completeness, the fourth-order implicit Runge-Kutta-Fehlberg scheme [15] given below is also considered.
Runge-Kutta-Fehlberg method:

$$\phi^{n+1} = \phi^n + \frac{\Delta t}{2}\left(\frac{5}{18}\ell^{(1)} + \frac{4}{9}\ell^{(2)} + \frac{5}{18}\ell^{(3)}\right) \tag{2.25}$$

Note that the above three weighting coefficients $\ell^{(i)}(i = 1\text{–}3)$ are implicitly coupled as follows:

$$\ell^{(1)} = F\left[t^n + \frac{1}{2}\left(1 - \frac{\sqrt{3}}{5}\right)\Delta t, \phi^n + \frac{5}{36}\ell^{(1)} + \left(\frac{2}{9} - \frac{1}{\sqrt{15}}\right)\ell^{(2)} + \left(\frac{5}{36} - \frac{1}{2\sqrt{15}}\right)\ell^{(3)}\right] \tag{2.26}$$

$$\ell^{(2)} = F\left[t^n + \frac{1}{2}\Delta t, \phi^n + \left(\frac{5}{36} + \sqrt{\frac{15}{24}}\right)\ell^{(1)} + \frac{2}{9}\ell^{(2)} + \left(\frac{5}{36} - \sqrt{\frac{15}{24}}\right)\ell^{(3)}\right] \tag{2.27}$$

$$\ell^{(3)} = F\left[t^n + \frac{1}{2}\left(1 + \frac{\sqrt{3}}{5}\right)\Delta t, \phi^n + \left(\frac{5}{36} + \frac{1}{2\sqrt{15}}\right)\ell^{(1)} + \left(\frac{2}{9} + \frac{1}{\sqrt{15}}\right)\ell^{(2)} + \frac{5}{36}\ell^{(3)}\right] \tag{2.28}$$

Due to the implicit nature of the developed method, the value of ϕ may be computationally expensive to calculate from the matrix equations. The fourth-order explicit schemes, namely, the explicit Runge-Kutta scheme [12], the Adams-Bashforth (open-type) scheme [14], and the Gear (open-type) scheme, are therefore considered in the current assessment study and are expressed as follows.

Runge-Kutta method:

$$\phi^{n+1} = \phi^n + \frac{\Delta t}{6}(k^{(1)} + 2k^{(2)} + 2k^{(3)} + k^{(4)}) \tag{2.29}$$

where $k^{(1)} = F(t^n, \phi^n)$, $k^{(2)} = F[t^n + (\Delta t/2), \phi^n + (\Delta t/2)k^{(1)}]$, $k^{(3)} = F[t^n + (\Delta t/2), \phi^n + (\Delta t/2)k^{(2)}]$, and $k^{(4)} = F(t^n + \Delta t, \phi^n + \Delta t k^{(3)})$.

Adams-Bashforth method:

$$\phi^{n+1} = \phi^n + \frac{\Delta t}{24}(55F^n - 59F^{n-1} + 37F^{n-2} - 9F^{n-3}) \tag{2.30}$$

Gear method:

$$\phi^{n+1} = \frac{1}{3}(-10\phi^n + 18\phi^{n-1} - 6\phi^{n-2} + \phi^{n-3}) + 4\Delta t F^n \tag{2.31}$$

By using the above three explicit schemes one can avoid matrix calculation and thus there is no storage problem for the coefficient matrix. This advantage is, however, shadowed by the accompanying Fourier stability limitation. The trade-off between the stability restriction and the matrix storage/calculation limitation motivated the assessment study.

3. FOURTH-ORDER SPATIAL SCHEME

As Eqs. (2.19)–(2.20) reveal, the accuracy of the solution obtained from Eq. (2.1) using the present semidiscretization scheme depends partly on the spatial

discretization scheme employed for the following convection-diffusion-reaction equation:

$$\bar{u}\phi_x + \bar{v}\phi_y - \bar{k}\nabla^2\phi + \bar{c}\phi = \bar{f} \tag{3.1}$$

In the above equation,

$$(\bar{u}, \bar{v}, \bar{k}, \bar{c}, \bar{f}) = \left(\frac{u\,\Delta t}{2}, \frac{v\,\Delta t}{2}, \frac{k\,\Delta t}{2}, 0, \phi^{n+1/2} - \phi^{n+1}\right) \quad \text{and}$$
$$\left(\frac{u\,\Delta t}{6}, \frac{v\,\Delta t}{6}, \frac{k\,\Delta t}{6}, 1, \phi^{n+5/6}\right)$$

for Eqs. (2.19) and (2.20), respectively. For simplicity, Eq. (3.1) is solved subject to the boundary solution $\phi = \mathbf{g}$. For efficiency, Eq. (3.1) is solved using the operator splitting scheme of Peaceman and Rachford [25]. As a result, calculation of ϕ involves solving the following predictor and corrector equations:

$$\bar{u}\phi_x^* - \bar{k}\phi_{xx}^* + \bar{c}\phi^* = f_1 \tag{3.2}$$

$$\bar{v}\phi_y^{n+1} - \bar{k}\phi_{yy}^{n+1} + \bar{c}\phi^{n+1} = f_2 \tag{3.3}$$

where $f_1 = \bar{f} - \bar{v}\phi_y^n + \bar{k}\phi_{yy}^n$ and $f_2 = \bar{f} - \bar{u}\phi_x^* + \bar{k}\phi_{xx}^*$. The calculation of ϕ from Eq. (3.1) starts with prescribing the value for f_1 using the most updated value of ϕ. This is followed by calculating ϕ^* using the nodally exact one-dimensional CDR scheme, which will be detailed below. Upon obtaining the value of ϕ^*, f_2 is computed and then ϕ^{n+1} is obtained using a nodally exact CDR scheme similar to the predictor step. This sweep-by-sweep calculation terminates until the user's specified tolerance is reached.

Based on Eqs. (3.2)–(3.3), we proceed to solve the following CDR equation:

$$u\phi_x - k\phi_{xx} + c\phi = f \tag{3.4}$$

Comparing Eq. (3.4) with Eqs. (3.2) and (3.3), it can be noted that $(u, k, c, f) = (\bar{u}, \bar{k}, \bar{c}, f_1)$ and $(\bar{v}, \bar{k}, \bar{c}, f_2)$. Discretization of Eq. (3.4) involves employing the general solution for Eq. (3.4), namely, $\phi(x) = c_1\, e^{\lambda_1 x} + c_2\, e^{\lambda_2 x} + f/c$, where c_1 and c_2 are constants. Substituting this equation into Eq. (3.4), we obtain

$$(\lambda_1, \lambda_2) = \left(\frac{u + \sqrt{u^2 + 4ck}}{2k}, \frac{u - \sqrt{u^2 + 4ck}}{2k}\right)$$

The discrete equation at an interior node j is expressed as

$$\left(-\frac{u}{2h} - \frac{\alpha k}{h^2} + \frac{c}{6}\right)\phi_{j-1} + 2\left(\frac{\alpha k}{h^2} + \frac{c}{3}\right)\phi_j + \left(\frac{u}{2h} - \frac{\alpha k}{h^2} + \frac{c}{6}\right)\phi_{j+1} = f \tag{3.5}$$

In the above discrete equation, h denotes the mesh size. By substituting the exact solutions $\phi_j = c_1 e^{\lambda_1 x_j} + c_2 e^{\lambda_2 x_j} + f/c$, $\phi_{j+1} = c_1 e^{\lambda_1 h} e^{\lambda_1 x_j} + c_2 e^{\lambda_2 h} e^{\lambda_2 x_j} + f/c$, and

$\phi_{j-1} = c_1\ e^{-\lambda_1 h} e^{\lambda_1 x_j} + c_2 e^{-\lambda_2 h} e^{\lambda_2 x_j} + f/c$ into Eq. (3.5), α can be derived analytically in terms of $\mathrm{Pe} = uh/k$ and $R = ch/u$ as

$$\alpha = \frac{(\mathrm{Pe}\,R/3) + (\mathrm{Pe}R/6)\ \cosh(\overline{\lambda_1})\cosh(\overline{\lambda_2}) + (\mathrm{Pe}/2)\ \sinh(\overline{\lambda_1})\cosh(\overline{\lambda_2})}{\cosh(\overline{\lambda_1})\cosh(\overline{\lambda_2}) - 1} \tag{3.6}$$

where $(\overline{\lambda_1}, \overline{\lambda_2}) = (\mathrm{Pe}/2, \sqrt{(\mathrm{Pe}/2)^2 + \mathrm{Pe}\,R})$. Note that the resulting prediction error stems solely from f.

The simulation quality for Eq. (2.1) depends solely on how ϕ_x, ϕ_y, ϕ_{xx}, and ϕ_{yy} shown in the source term are approximated. To obtain a physically rational approximation of ϕ_x, for example, we apply the following fourth-order-accurate, wavenumber-extended, upwind-biased finite-differencing scheme [26] for the positive-velocity case $u_j > 0$; that for the negative-velocity case $u_j < 0$ is analogous to the former scheme.

$$\begin{aligned}\phi_x|_j = \frac{1}{h}(&-0.055453\,\phi_{j-3} + 0.360600\,\phi_{j-2} - 1.221201\,\phi_{j-1} \\ &+ 0.554534\,\phi_j + 0.389400\,\phi_{j+1} - 0.027880\,\phi_{j+2})\end{aligned} \tag{3.7}$$

Note that $\phi_i (i < j)$ at the upstream side of the nodal point j should be considered in the convection-dominated case. At the two boundary nodes ($j = 1$ and $j_{\max}$) and at the nodes next to the two most left and right interior points, the following expressions for ϕ_x are applied:

$$\phi_x|_{\text{left}} = \frac{1}{12h}\begin{cases}(-25\,\phi_j + 48\,\phi_{j+1} - 36\,\phi_{j+2} + 16\,\phi_{j+3} - 3\,\phi_{j+4}) & j = 1 \\ (-3\,\phi_{j-1} - 10\,\phi_j + 18\,\phi_{j+1} - 6\,\phi_{j+2} + \phi_{j+3}) & j = 2, 3\end{cases} \tag{3.8}$$

$$\phi_x|_{\text{right}} = \frac{1}{12h}\begin{cases}(25\phi_j - 48\phi_{j-1} + 36\phi_{j-2} - 16\phi_{j-3} + 3\phi_{j-4}) & j = j_{\max} \\ (-\phi_{j-3} + 6\phi_{j-2} - 18\phi_{j-1} + 10\phi_j + 3\phi_{j+1}) & j = j_{\max} - 1,\ j_{\max} - 2\end{cases} \tag{3.9}$$

On physical grounds, ϕ_{xx} is approximated by employing the following fourth-order-accurate centered scheme:

$$\phi_{xx}|_j = \frac{1}{12h^2}(-\phi_{j-2} + 16\phi_{j-1} - 30\phi_j + 16\phi_{j+1} - \phi_{j+2}) \tag{3.10}$$

Similarly, for the approximation of ϕ_{xx} at and adjacent to the two end boundaries, the following equations are employed:

$$\phi_{xx}|_{\text{left}} = \frac{1}{12h^2}\begin{cases}(35\phi_j - 104\phi_{j+1} + 114\phi_{j+2} - 56\phi_{j+3} + 11\phi_{j+4}) & j = 1 \\ (11\phi_{j-1} - 20\phi_j + 6\phi_{j+1} + 4\phi_{j+2} - \phi_{j+3}) & j = 2, 3\end{cases} \tag{3.11}$$

$$\phi_{xx}|_{right} = \frac{1}{12h^2}\begin{cases}(35\phi_j - 104\phi_{j-1} + 114\phi_{j-2} - 56\phi_{j-3} + 11\phi_{j-4}) & j = j_{\max} \\ (-\phi_{j-3} + 4\phi_{j-2} + 6\phi_{j-1} - 20\phi_j + 11\phi_{j+1}) & j = j_{\max} - 1,\ \ j_{\max} - 2\end{cases} \tag{3.12}$$

4. FUNDAMENTAL STUDIES

Theoretical study of the multistep schemes detailed in Sections 2 and 3 is carried out using their equivalent one-step equation. For this reason, Eqs. (2.14) and (2.15) are first added, and then the definitions given in (2.12)–(2.13) are employed to derive the following one-step implicit equation:

$$\phi^{n+1} = \frac{1}{2}(\phi^{n+1/6} + \phi^{n+5/6}) + \frac{\Delta t}{12}(F^{n+1} - F^n + 3F^{n+1/6} + 3F^{n+5/6}) \tag{4.1}$$

Subject to the initial solution $\phi(x, t = 0) = \exp(ik_m x)$, the model equation

$$\phi_t + u\phi_x - k\phi_{xx} + c\phi = 0 \tag{4.2}$$

can be easily shown to have an exact solution given by

$$\phi(x, t) = \exp[-(kk_m^2 + c)t] \exp[ik_m(x - ut)] \tag{4.3}$$

In the above expression, k_m denotes the wavenumber. Denoting $h(\equiv \Delta x)$ as the mesh size and Δt as the time increment, the proposed discrete equation for (4.2) is shown to be equivalent to

$$\begin{aligned} A_1\phi_{j-1}^{n+1} + A_2\phi_j^{n+1} + A_3\phi_{j+1}^{n+1} = {} & 6\left(\phi_j^{n+1/6} + \phi_j^{n+5/6}\right) - \Delta t(-u\phi_x^n + k\phi_{xx}^n - c\phi^n) \\ & + 3\Delta t\left(-u\phi_x^{n+1/6} + k\phi_{xx}^{n+1/6} - c\phi^{n+1/6}\right) \\ & + 3\Delta t\left(-u\phi_x^{n+5/6} + k\phi_{xx}^{n+5/6} - c\phi^{n+5/6}\right) \end{aligned} \tag{4.4}$$

The tridiagonal coefficients A_1, A_2, and A_3, which are written in terms of $v = u\,\Delta t/h$ and $R = ch/u$, are expressed as

$$A_1 = -\frac{\overline{\alpha}\nu}{\mathrm{Pe}} - \frac{\nu}{2} + \frac{\nu R + 12}{6} \qquad A_2 = 2\left(\frac{\overline{\alpha}\nu}{\mathrm{Pe}} + \frac{\nu R + 12}{3}\right) \qquad A_3 = -\frac{\overline{\alpha}\nu}{\mathrm{Pe}} + \frac{\nu}{2} + \frac{\nu R + 12}{6}$$

According to the definition of $\mathrm{Pe}(= uh/k)$, $\overline{\alpha}$ is derived theoretically as

$$\overline{\alpha} = h^2\left\{\frac{[(\nu R+12)/3] + [(\nu R+12)/6]\cosh(\overline{\lambda_1}^*)\cosh(\overline{\lambda_2}^*) + (\nu/2)\sinh(\overline{\lambda_1}^*)\cosh(\overline{\lambda_2}^*)}{\cosh(\overline{\lambda_1}^*)\cosh(\overline{\lambda_2}^*) - 1}\right\} \tag{4.5}$$

where $\overline{\lambda_1}^* = \mathrm{Pe}/2$ and $\overline{\lambda_2}^* = [(\mathrm{Pe}/2)^2 + \mathrm{Pe}(R + 12/\nu)]^{1/2}$.

Owing to the discretized amplitude and phase errors, the exact solution for the discrete equation (4.4) is assumed to take the following form:

$$\phi(x, t) = \exp\left[-(kk_m^2 + c)\frac{k_r}{\beta^2}t\right] \exp\left[ik_m\left(x - u\frac{k_i}{\beta}t\right)\right] \tag{4.6}$$

The modified wavenumber shown above is expressed as $\beta = k_m h$. The dispersion analysis of Eq. (4.4) starts by substituting ϕ_j and $\phi_{j\pm1}$, which are obtained from Eq. (4.6), into equation (4.4). After some algebra, the introduced k_r and k_i shown in Eq. (4.6) for measuring the respective amplitude and phase errors are derived as

$$k_r = -\frac{p}{\nu[(1/\mathrm{Pe}) + (R/\beta^2)]} \tag{4.7}$$

$$k_i = \frac{q}{\nu} \tag{4.8}$$

where

$$p = \ln\left[\sqrt{\left(\frac{f_1 \cdot a - f_2 \cdot b}{a^2 + b^2}\right)^2 + \left(\frac{f_1 \cdot b + f_2 \cdot a}{a^2 + b^2}\right)^2}\right] \tag{4.9}$$

$$q = \tan^{-1}\left(\frac{f_1 \cdot b + f_2 \cdot a}{f_1 \cdot a - f_2 \cdot b}\right) \tag{4.10}$$

In the above two equations, $a = (A_1 + A_3)\cos\beta + A_2$, $b = (A_1 - A_3)\sin\beta$, where

$$f_1 = (k_1 + 6)\left(e^{(1/6)p}\cos\frac{1}{6}q + e^{(5/6)p}\cos\frac{5}{6}q\right) + k_1 - k_2\left(e^{(1/6)p}\sin\frac{1}{6}q + e^{(5/6)p}\sin\frac{5}{6}q\right) \tag{4.11}$$

$$f2 = (k_2 + 6)\left(e^{(1/6)p}\sin\frac{1}{6}q + e^{(5/6)p}\sin\frac{5}{6}q\right) - k_2 + k_1\left(e^{(1/6)p}\cos\frac{1}{6}q + e^{(5/6)p}\cos\frac{5}{6}q\right) \tag{4.12}$$

In Eqs. (4.11) and (4.12), k_1 and k_2 are expressed as

$$k_1 = B_1\cos 3\beta + B_2\cos 2\beta + B_3\cos\beta + B_4 + B_5\cos\beta + B_6\cos 2\beta \tag{4.13}$$

$$k_2 = B_1\sin 3\beta + B_2\sin 2\beta + B_3\sin\beta - B_5\sin\beta - B_6\sin 2\beta \tag{4.14}$$

The expressions for $B_1 - B_6$ are detailed in [27].

To reveal clearly the dissipative and dispersive errors, k_r and k_i are plotted against Pe, $R(\equiv ch/u)$, and ν in Figure 1. For the case considered at $R = 1$, it is known that k_r and k_i agree perfectly with β^2 and β, respectively, in the small-modified-wavenumber range. The larger the modified wavenumber, the less satisfactory agreement is observed. Note that the proposed scheme is of the dissipative type since k_r is seen to have the positive value in the entire wavenumber range. For the sake of comparison with the other schemes investigated, k_r and k_i are also plotted in Figure 2.

In Figure 3, the numerical group velocity $C_g(\equiv dw/dk_m)$ (in which w is obtained from the dispersion relation) is observed to have a magnitude smaller than the analytic propagation speed. The proposed scheme is thus classified to be phase-lagging. For the sake of completeness, dispersion analysis of the investigated schemes is also conducted. The derived s_1 and s_2 shown in $k_r = \ln(\sqrt{s_1^2 + s_2^2})$ and $k_i = \tan^{-1}(s_2/s_1)$ are detailed in [27].

After the fundamental study of the proposed fourth-order scheme, a Fourier (or von Neumann) stability analysis is conducted so as to reveal its amplification factor. Let $\beta = (2\pi m/2L)h$ $(m = 0, 1, 2, 3, \ldots, M)$, h being the grid size, and $2L$ being the period of fundamental frequency $(m = 1)$; the amplification factor $|G|(\equiv |\phi_j^{n+1}/\phi_j^n|)$ is derived in terms of p and q shown in Eqs. (4.9) and (4.10), where $G = e^p(\cos q + i\sin q)$. From Figure 4, it is observed that the proposed scheme is unconditionally stable. The amplification factor shown above can be rewritten in exponential form as $G = |G|e^{i\theta}$, where the phase angle θ is defined as

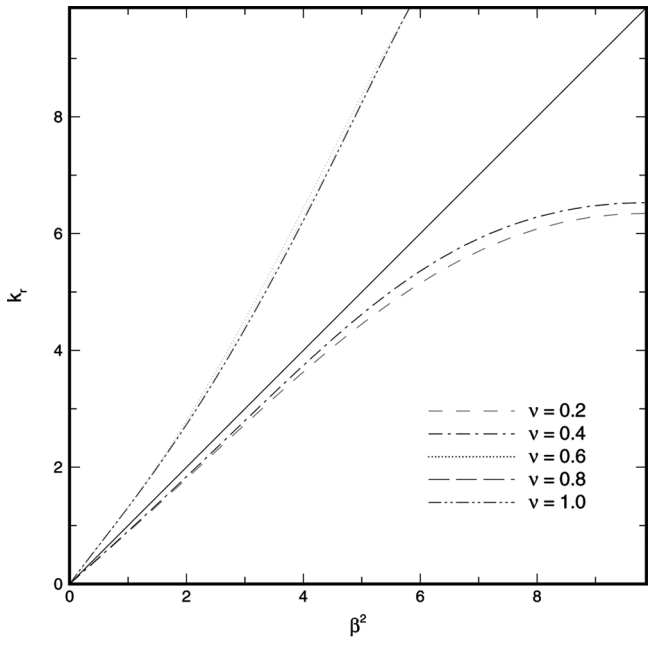

(*a*)

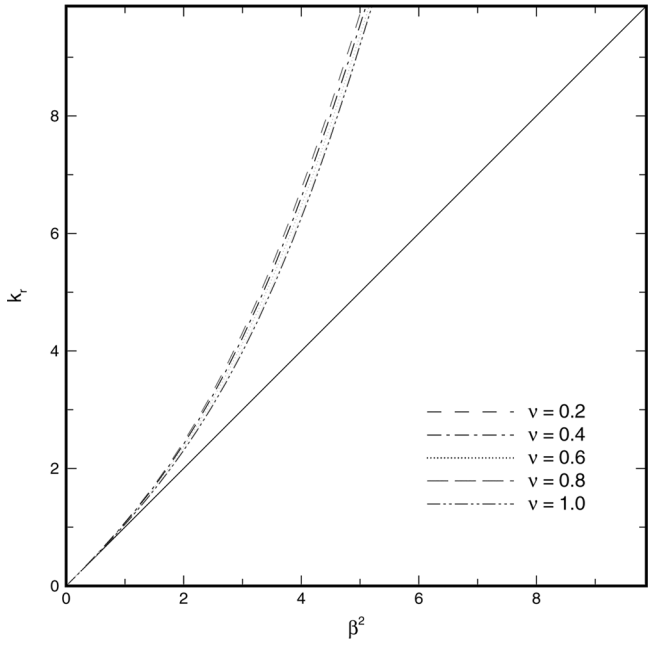

(*b*)

Figure 1. Plots of k_r and k_i versus β^2 and β for the case with $R = 1$ and five chosen magnitudes of ν: (*a*) k_r for Pe = 5; (*b*) k_r for Pe = 100; (*c*) k_i for Pe = 5; (*d*) k_i for Pe = 100. Note that β is the modified wave-number.

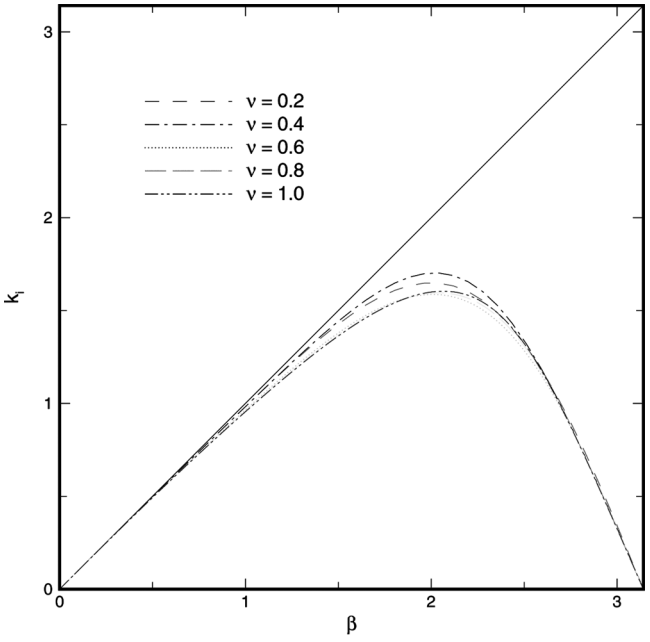

(*c*)

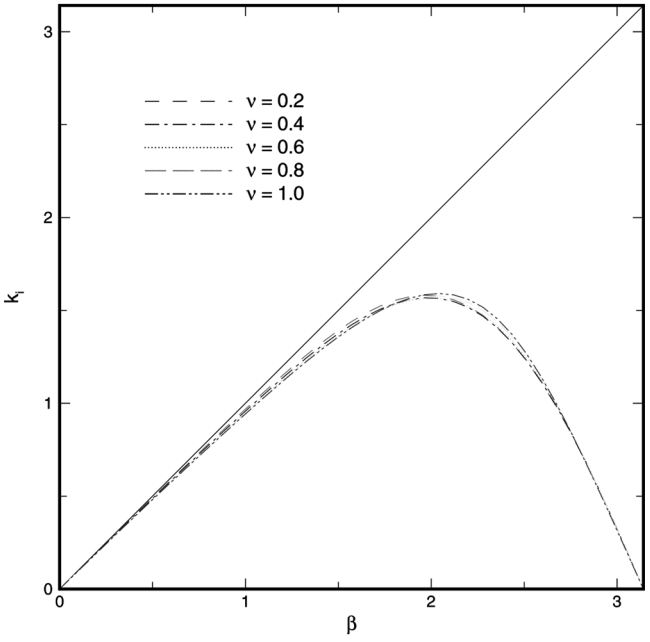

(*d*)

Figure 1. Continued.

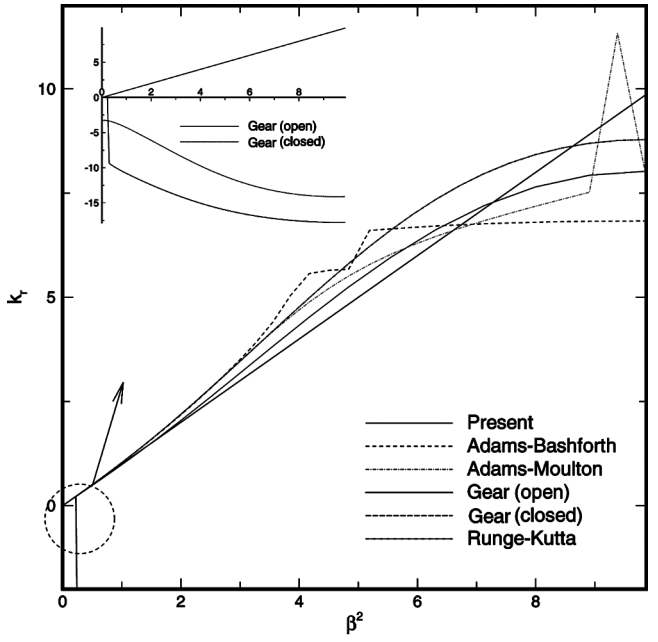

(*a*)

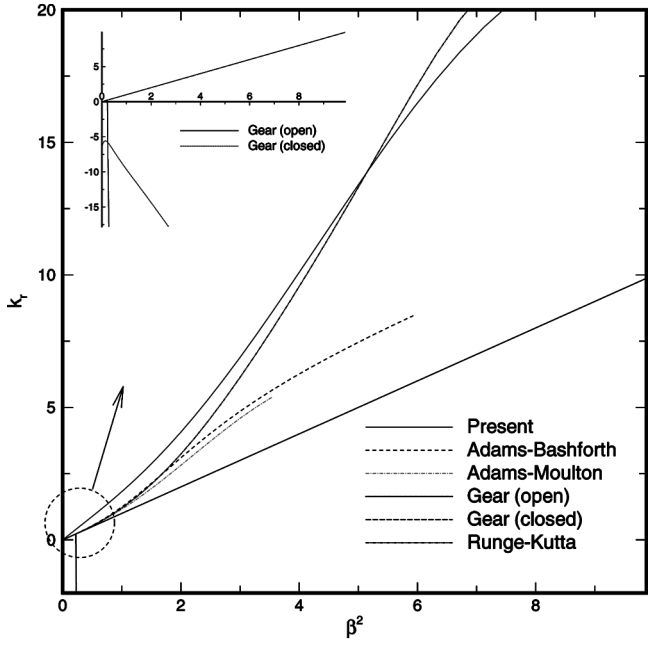

(*b*)

Figure 2. Plots of k_r and k_i versus β^2 and β for the case with $R = 1$: (*a*) k_r for $\nu = 0.2$, Pe $= 2$; (*b*) k_r for $\nu = 0.5$, Pe $= 10$; (*c*) k_i for $\nu = 0.2$, Pe $= 2$; (*d*) k_i for $\nu = 0.5$, Pe $= 10$.

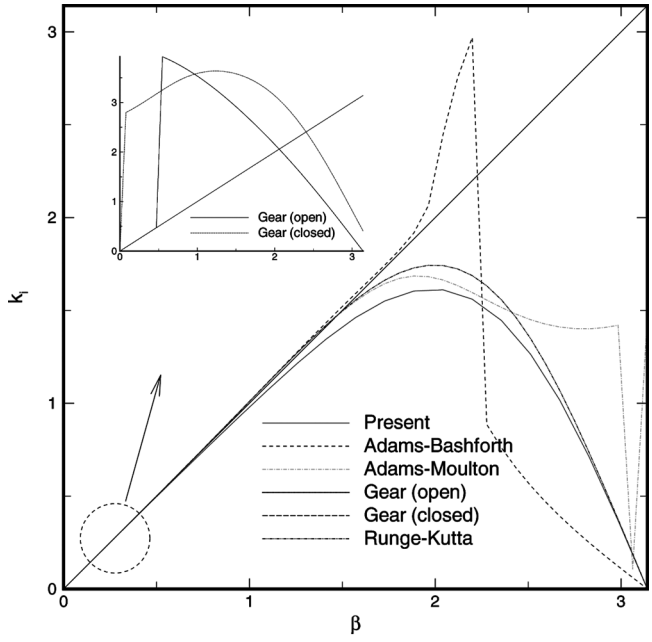

(*c*)

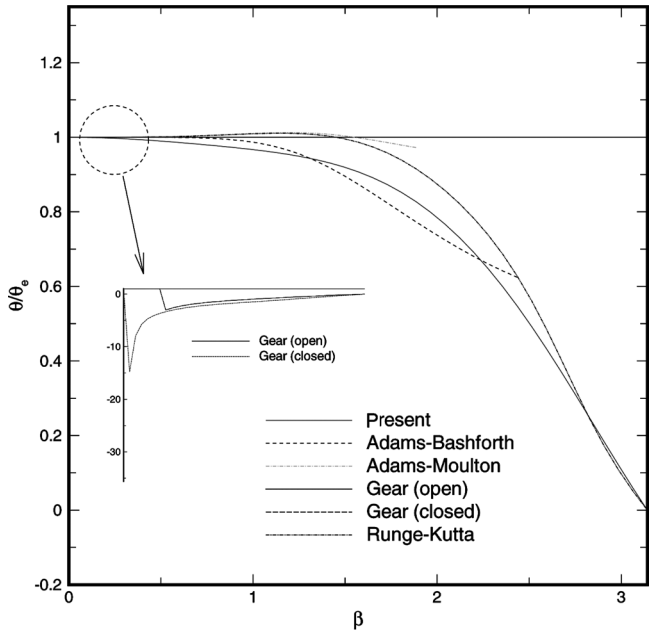

(*d*)

Figure 2. Continued.

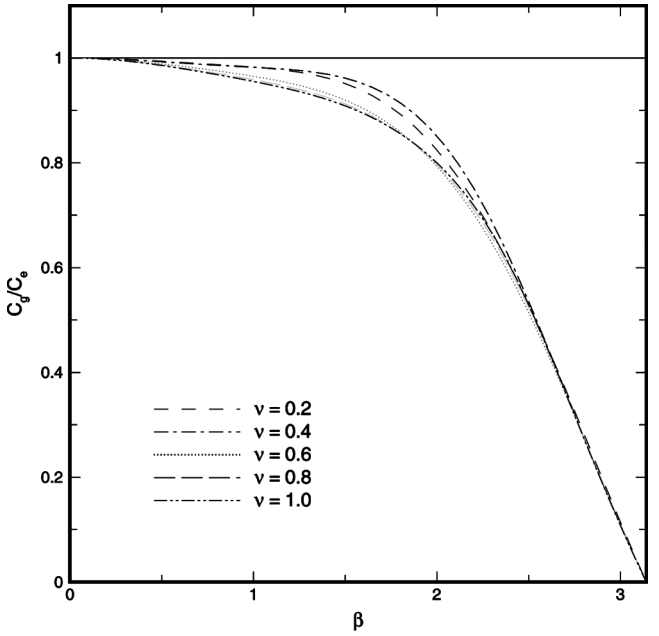

(*a*)

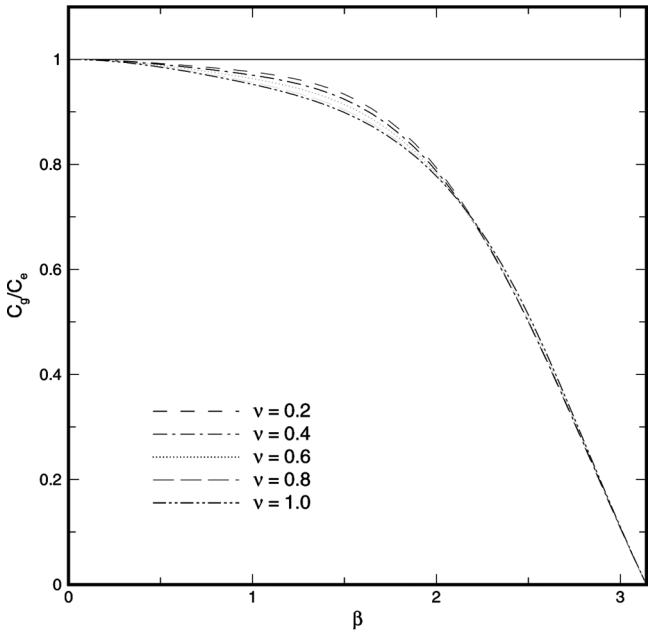

(*b*)

Figure 3. Plots of group velocity ratio C_g/C_e versus modified wavenumber β for the case with $R = 1$ and five chosen magnitudes of ν: (*a*) Pe = 5; (*b*) Pe = 100. Note that C_g and C_e are the numerical and exact group velocities, respectively.

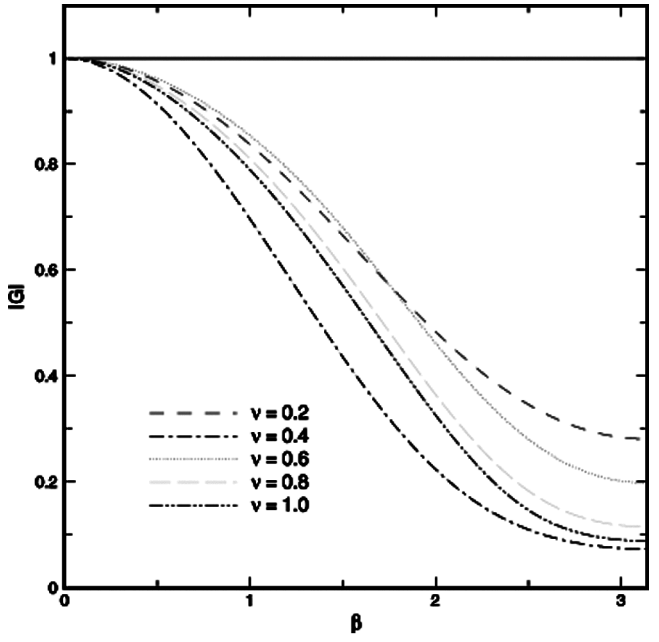

(*a*)

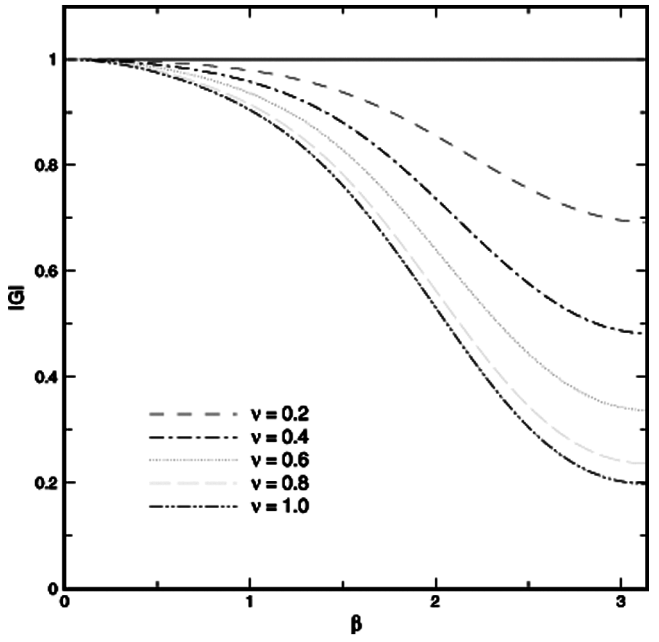

(*b*)

Figure 4. Plots of amplification factor $|G|$ versus modified wavenumber β for the case with $R = 1$ and five chosen magnitudes of ν: (*a*) Pe = 5; (*b*) Pe = 100.

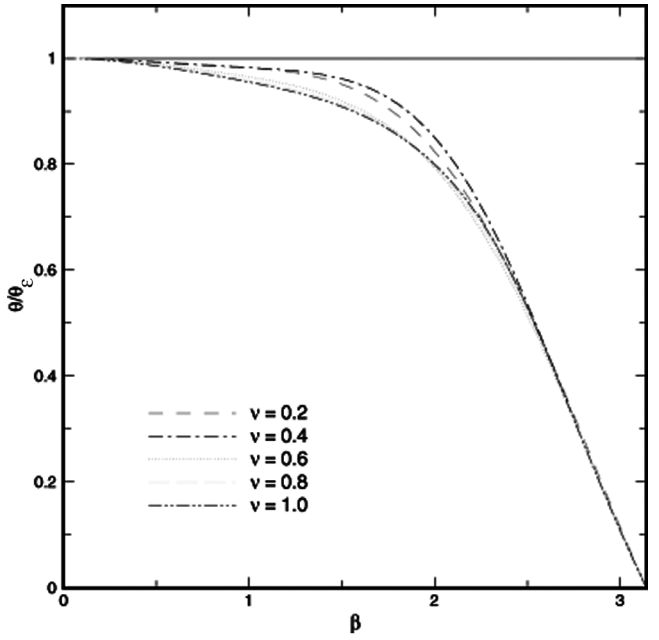

(*a*)

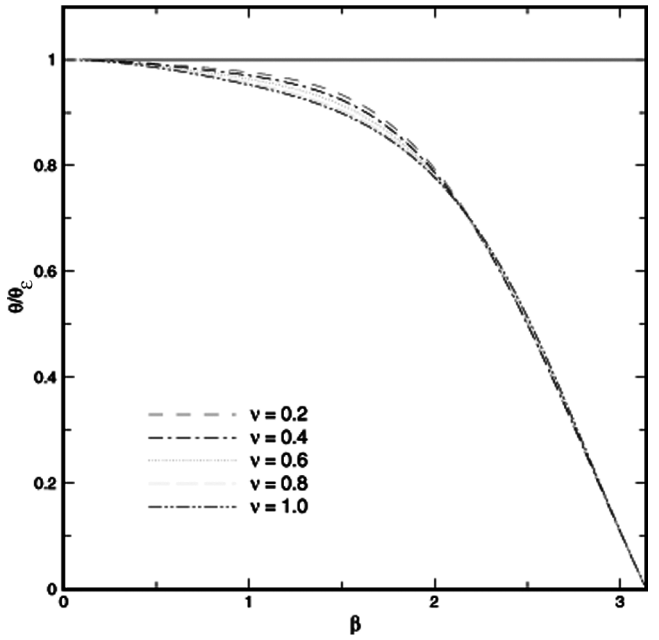

(*b*)

Figure 5. Plots of phase angle ratio θ/θ_e versus modified wavenumber β for the case with $R = 1$ and five chosen magnitudes of ν: (*a*) Pe = 5; (*b*) Pe = 100.

$\theta = \tan^{-1} |\mathrm{Im}(G)/\mathrm{Re}(G)|$. To study the θ variation with respect to the dimensionless numbers $\mathrm{Pe} = uh/k$, $R = ch/u$, and $\nu = u\,\Delta t/h$, the exact phase angle θ_e, which is $-\nu\beta$, is derived. The ratio θ/θ_e plotted in terms of β is shown in Figure 5. The reader can refer to [27] for the rest of the investigated schemes.

5. NUMERICAL STUDIES

5.1. One-Dimensional Problems

The first test problem is the diffusion-reaction equation defined in $0 \le x \le 1$:

$$-k\phi_{xx} + c\phi = f \tag{5.1}$$

$$\phi(0) = \phi(1) = f(0) \tag{5.2}$$

where

$$f(x) = \begin{cases} -0.5\,x & x \le 0.5 \\ 0.5 & x > 0.5 \end{cases} \tag{5.3}$$

It is well known that this problem has the interior layer developed at $x = 0.5$ and the boundary layer formed at $x = 1$ according to the solution derived as follows [28]:

$$\phi = 0.25(A + B)\left[\exp\left(-\frac{0.5 - x}{\sqrt{k}}\right) - \exp\left(\frac{-0.5 + x}{\sqrt{k}}\right)\right] - 0.5x \qquad x \le 0.5 \tag{5.4}$$

and

$$\phi = 0.25(A - B)\exp\left(-\frac{1}{2\sqrt{k}}\right)\left[\exp\left(-\frac{x-1}{\sqrt{k}}\right) - \exp\left(-\frac{1-x}{\sqrt{k}}\right)\right] + 0.5\left[1 - \exp\left(-\frac{1-x}{\sqrt{k}}\right)\right] \qquad x \le 0.5 \tag{5.5}$$

In the above equations, $A = [\sqrt{k} - \exp(-1/2\sqrt{k})]/[1 + \exp(-1/\sqrt{k})]$ and $B = [1.5 - \exp(-1/2\sqrt{k})]/[1 - \exp(-1/\sqrt{k})]$. For the case considered at $k(= 10^{-2}, 10^{-8})$, $c = 1$, and $h = \frac{1}{41}$, the computed results shown in Figure 6 are found to reproduce the sharply varying analytic solution. In Table 1 the solution quality of the proposed equal-order finite-difference scheme is clearly shown to outperform the scheme of Miller et al. [28].

Having verified the proposed steady-state scheme, we now turn our attention to the time-dependent convection-diffusion equation in $0 \le x \le 1$:

$$\phi_t + u\phi_x - k\phi_{xx} + c\phi = 0 \tag{5.6}$$

Subject to $\phi(x, t = 0) = x^2$, the exact solution for the case with $u = 1$, $k = x$, and $c = 1$ takes the form $\phi(x, t) = x^2 e^{-t}$. Calculations were also carried out on the continuously refined grid sizes of $h = \frac{1}{11}, \frac{1}{21}, \frac{1}{41}, \frac{1}{81}$, and $\frac{1}{101}$. This was followed by plotting

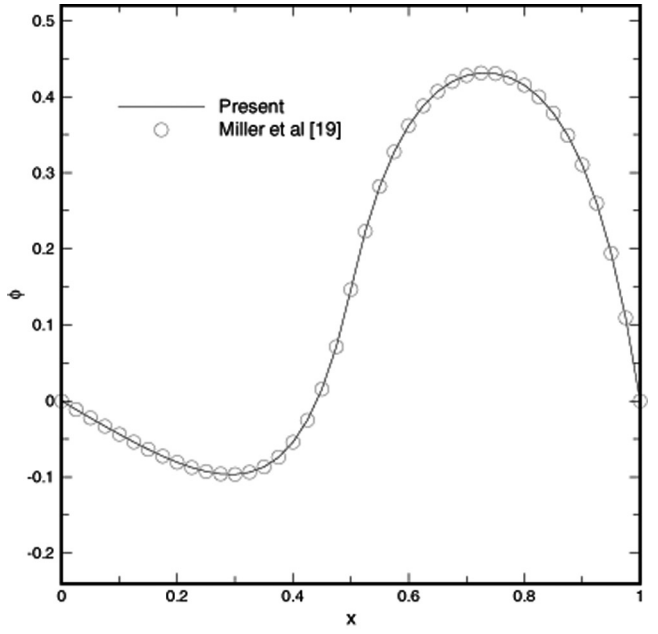

(*a*)

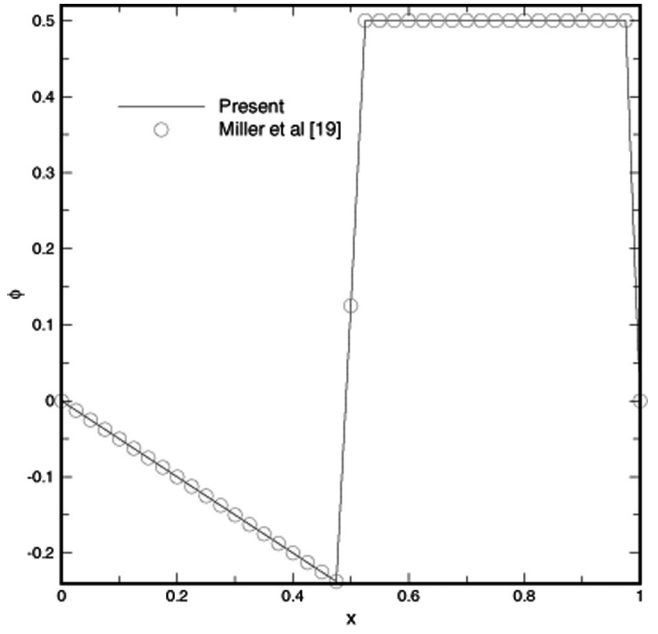

(*b*)

Figure 6. Simulated ϕ profiles for the problem defined in (5.1)–(5.3), investigated at two values of k: (*a*) $k = 10^{-2}$; (*b*) $k = 10^{-8}$.

Table 1. Simulated maximum pointwise errors for Eqs. (5.1)–(5.3) investigated at five discussion coefficients of k and N nodal points

		$N = 8$	16	32	64	128	256	512	1,024
$k = 1$	Present	2.67E-3	6.58E-4	1.63E-4	4.07E-5	1.01E-5	2.53E-6	6.34E-7	1.58E-7
	Miller et al. [28]	3.78E-3	1.66E-3	7.95E-4	3.90E-4	1.93E-4	9.63E-5	4.80E-5	2.40E-5
10^{-2}	Present	9.34E-3	2.19E-3	5.39E-4	1.33E-4	3.33E-5	8.33E-6	2.08E-6	5.20E-7
	Miller et al. [28]	9.42E-3	3.75E-3	1.72E-3	8.25E-4	4.05E-4	2.01E-4	9.99E-5	4.98E-5
10^{-4}	Present	5.48E-5	5.35E-5	4.38E-5	2.74E-5	1.46E-5	7.46E-6	3.75E-6	1.87E-6
	Miller et al. [28]	9.49E-3	2.06E-3	6.45E-4	2.49E-4	1.08E-4	5.04E-5	2.43E-5	1.19E-5
10^{-6}	Present	0.00E + 0	0.00E + 0	2.77E-17	5.55E-17	2.77E-17	5.55E-17	8.32E-17	2.77E-17
	Miller et al. [28]	8.39E-3	4.86E-3	2.69E-3	1.37E-3	6.89E-4	3.45E-4	1.72E-4	8.62E-5
10^{-8}	Present	0.00E + 0	0.00E + 0	0.00E + 0	0.00E + 0	0.00E + 0	2.77E-17	0.00E + 0	0.00E + 0
	Miller et al. [28]	1.89E-2	9.09E-3	4.29E-3	2.04E-3	9.95E-4	4.90E-4	2.43E-4	1.21E-4

$\log(\mathrm{err}_1/\mathrm{err}_2)$ against $\log(h_1/h_2)$ for the L_2-error norms err_1 and err_2 obtained at two continuously refined grids h_1 and h_2. As Figure 7 shows, the rates of convergence are obtained as 3.941/3.966 (temporal/spatial), which agree fairly well with the theoretical rates of convergence, using the proposed scheme. Assessment of the currently investigated schemes is made using the simulated results $\phi(x, t = 1)$ cast in the L_2-error norms tabulated in Table 2.

The validation is followed by solving the nonlinear transport equation $u_t + uu_x = u_{xx}$. This model equation is defined in $0 \le x \le 1$ and is solved subject to the following initial and boundary conditions:

$$u(x, 0) = \frac{(\pi/2)\,\sin(\pi x) + 2\pi \sin(2\pi x)}{1 + \frac{1}{4}\cos(\pi x) + \frac{1}{2}\cos(2\pi x)} \tag{5.7}$$

$$u(0, t) = u(1, t) = 0 \tag{5.8}$$

The resulting exact solution takes the following form [29]:

$$u(x, t) = \frac{(\pi/2)[\exp(-\pi^2 t)\sin(\pi x) + 4\exp(-4\pi^2 t)\sin(2\pi x)]}{1 + \frac{1}{4}\exp(-\pi^2 t)\cos(\pi x) + \frac{1}{2}\exp(-4\pi^2 t)\cos(2\pi x)} \tag{5.9}$$

All the calculations were carried out at $\Delta t = 10^{-3}$. Figure 8 shows the simulated L_2-error norms at $t = 1.0$ and the rates of convergence for the proposed scheme. The rapid convergence to the analytic solution (refer to Table 3) with a slope slightly larger than 4 (refer to Figure 8) is clearly demonstrated for the simulated results $\phi(x, t = 1)$.

5.2. Two-Dimensional Problems

The following pure advection (or inviscid Burgers') equation is considered first:

$$\phi_t + u\phi_x + v\phi_y = 0 \tag{5.10}$$

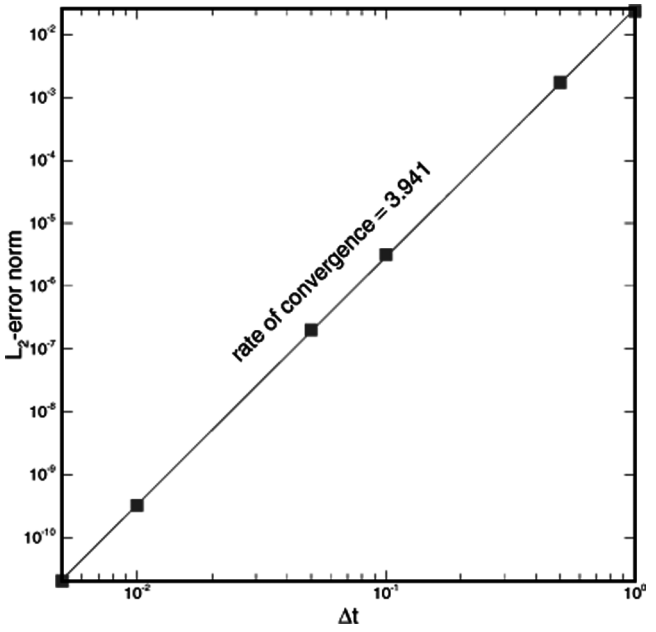

(*a*)

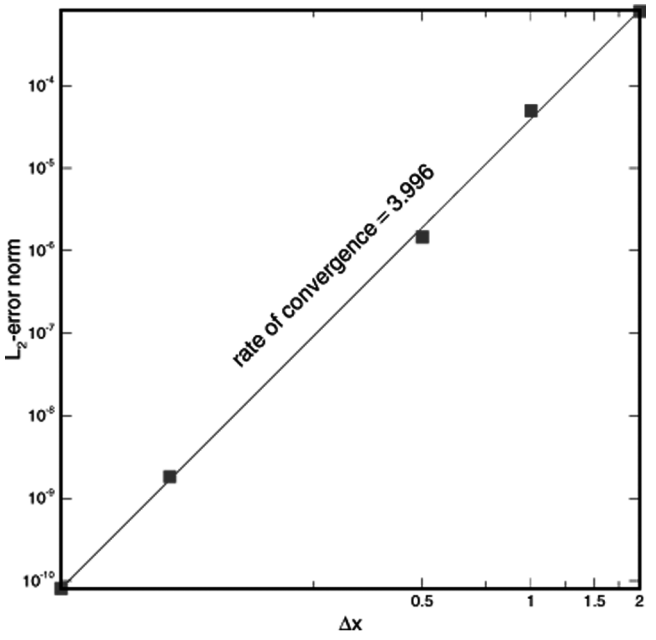

(*b*)

Figure 7. Simulated rates of convergence for the problem given by Eq. (5.6): (*a*) temporal rate of convergence; (*b*) spatial rate of convergence.

Table 2. Comparison of simulated L_2-norm errors for the solutions obtained at $\Delta t = 10^{-1}, 10^{-2}, 10^{-3}$, and 10^{-4} for the second problem in Section 5.1 (divergent solutions are marked with —)

Δt	Present Eq. (4.1)	AB Eq. (2.30)	Gear (open) Eq. (2.31)	RK Eq. (2.29)	AM Eqs. (2.21)–(2.22)	Gear (closed) Eqs. (2.23)–(2.24)	RKF Eq. (2.25)
10^{-1}	2.846E-5	2.233E-6	2.115E-6	1.890E-6	2.579E-7	1.174E-6	9.431E-5
10^{-2}	3.906E-7	—	—	—	—	—	5.141E-7
10^{-3}	3.907E-9	—	—	5.471E-10	—	—	3.081E-9
10^{-4}	3.206E-11	8.461E-9	—	2.129E-11	2.081E-9	9.974E-8	3.521E-11

where $(x, y, t) \in (0, 1) \times (0, 1) \times (0, 1)$. The problem to be investigated has a steep ramp function of width 0.01 and gradient 100. The analytic solution is given by

$$\phi(x, y, t) = 1.1 + \max[\min(\delta, 0), -1] \tag{5.11}$$

where $\delta = 100(0.1 - \frac{1}{2}(x + y) + t)$, $\Delta x = \Delta y = \frac{1}{41}$, and $\Delta t = 10^{-3}$. For the sake of assessment, all the predicted L_2-error norms at $t = 1$ are tabulated in Table 4 to show that the present scheme outperforms other schemes in terms of accuracy. Also, no oscillatory solution is observed near the steep ramp using the proposed scheme. In what follows, the required CPU times are also tabulated in $(\cdot)$ shown in the rest of tables.

The following convection-diffusion problem, known as the viscous Burgers' equation, defined in $(x, y, t) \in (0, 1) \times (0, 1) \times (0, 1)$, is then considered:

$$\phi_t + u\phi_x + v\phi_y = \nu\nabla^2\phi \tag{5.12}$$

The analytic solution is $\phi(x, y, t) = \overline{w}(x, t)\overline{w}(y, t)$, where $\overline{w}(x, t)$ is derived as

$$\overline{w}(x, t) = \frac{0.1A + 0.5B + C}{A + B + C} \tag{5.13}$$

In the above, $A = e^{-0.05(x-0.5+4.95t)/\nu}$, $B = e^{-0.25(x-0.5+0.75t)/\nu}$, and $C = e^{-0.5(x-0.375)/\nu}$. Solutions were obtained at $\Delta t = 10^{-3}$ and $\Delta x = \Delta y = \frac{1}{11}, \frac{1}{21}, \frac{1}{41}, \frac{1}{81}, \frac{1}{161}$ for the problem with $u = \overline{w}(x, t)$, $v = \overline{w}(y, t)$, and $\nu = 10^{-4}$. Convergence to the analytic solution with the theoretical rate is revealed by the solutions computed at several uniform meshes. Good agreement with the analytic solution is clearly demonstrated from the tabulated L_2-error norms for $\phi(x, y, t = 1)$ in Table 5. Unlike other solutions plotted in Figure 9, no oscillation is observed near the jump using the currently proposed scheme.

Finally, the following two-dimensional nonlinear viscous Burgers' equation is considered in $(x, y, t) \in (0, 1) \times (0, 1) \times (0.25, 1.25)$:

$$u_t + uu_x + uu_y = \nu\nabla^2 u \tag{5.14}$$

The initially smooth solution gradually evolves to produce the shocklike profile given below, due to the nonlinear term uu_x shown in (5.14) [30]:

$$u(x, y, t) = \frac{1}{1 + e^B} \tag{5.15}$$

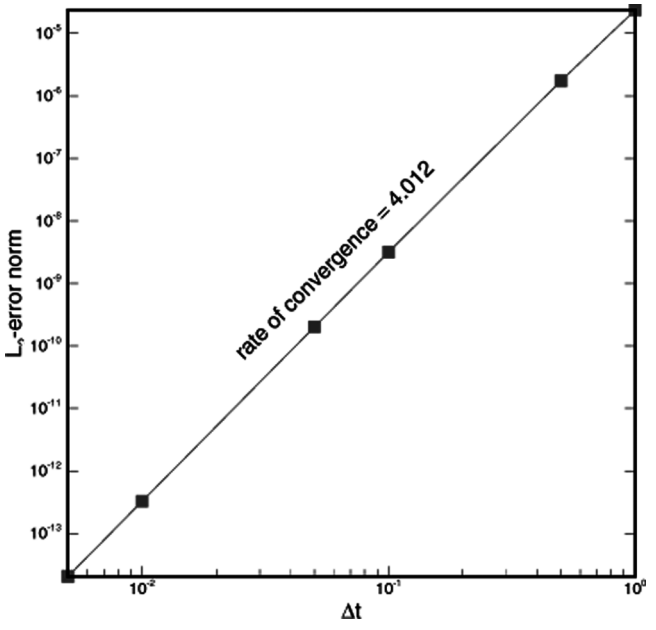

(*a*)

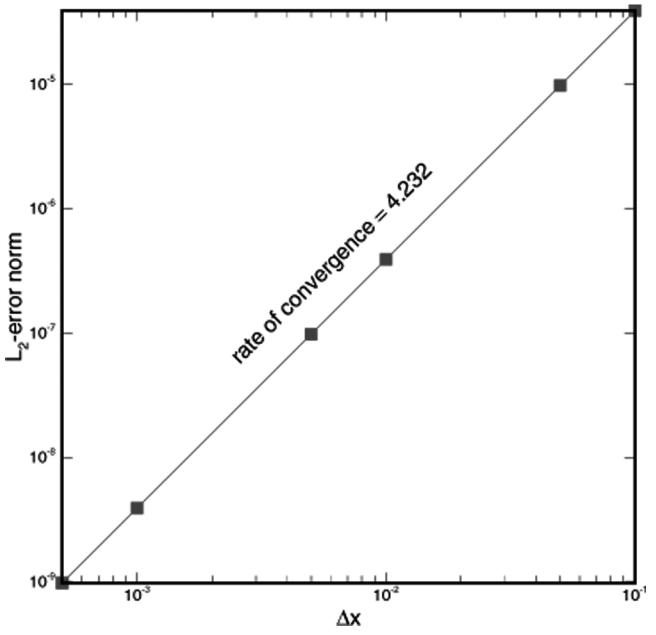

(*b*)

Figure 8. Simulated rates of convergence for the problem given by Eqs. (5.7)–(5.8): (*a*) temporal rate of convergence; (*b*) spatial rate of convergence.

Table 3. Comparison of simulated L_2-norm errors for the solutions obtained at $\Delta t = 10^{-1}$, 10^{-2}, 10^{-3}, and 10^{-4} for the third problem in Section 5.1 (divergent solutions are marked with —)

Δt	Present Eq. (4.1)	AB Eq. (2.30)	Gear (open) Eq. (2.31)	RK Eq. (2.29)	AM Eqs. (2.21)–(2.22)	Gear (closed) Eqs. (2.23)–(2.24)	RKF Eq. (2.25)
10^{-1}	1.045E-4	1.096E-1	4.359E-1	9.009E-3	1.628E-1	5.201E-2	2.760E-4
10^{-2}	1.054E-6	3.851E-8	—	1.025E-6	2.617E-7	3.335E-4	8.902E-7
10^{-3}	1.060E-8	2.136E-9	—	5.651E-9	4.401E-9	4.774E-5	8.408E-9
10^{-4}	1.501E-10	2.127E-10	—	2.428E-10	2.350E-10	4.955E-6	3.031E-10

Table 4 Comparison of simulated solutions obtained at $\Delta t = 10^{-1}$, 10^{-2}, 10^{-3}, and 10^{-4} for the first problem in Section 5.2 [(·) denotes CPU time]

Δt	Present Eq. (4.1)	AB Eq. (2.30)	Gear (open) Eq. (2.31)	RK Eq. (2.29)	AM Eqs. (2.21)–(2.22)	Gear (closed) Eqs. (2.23)–(2.24)	RKF Eq. (2.25)
10^{-1}	3.949E-01 (0.687)	4.351E+00 (0.781)	5.232E+00 (0.625)	8.330E+02 (0.625)	3.038E+01 (0.856)	4.644E+01 (0.656)	4.131E+00 (0.694)
10^{-2}	1.083E-02 (2.593)	3.882E-01 (2.234)	3.447E-01 (1.421)	4.138E-02 (2.125)	3.721E-01 (2.515)	4.357E-01 (1.781)	3.976E-02 (2.947)
10^{-3}	2.056E-03 (21.500)	4.249E-03 (16.890)	1.667E-02 (9.234)	3.853E-03 (17.062)	3.965E-03 (21.296)	1.940E-03 (14.015)	3.813E-03 (26.147)
10^{-4}	2.285E-04 (213.500)	4.544E-04 (216.828)	1.785E-03 (118.984)	4.543E-04 (218.500)	4.544E-04 (296.781)	2.225E-04 (180.750)	4.342E-04 (278.365)

where $B = x + y - t/\nu$. As a validation test, ν was chosen to be 10^{-4}. Three meshes, 21×21, 41×41, and 101×101, were used to calculate $u(x, y, t)$ under $\Delta t = 10^{-3}$ for the present problem with the initial and boundary conditions from Eq. (5.15). The results plotted in Figure 10 exhibit sharp solution profiles. To demonstrate that the proposed fourth-order-accurate scheme outperforms the other schemes investigated, the simulated L_2-error norms are summarized in Table 6.

6. CONCLUDING REMARKS

The aim of this study was to develop a fourth-order-accurate temporal scheme for the convection-diffusion transport equation investigated, without involving storage of several previously calculated solutions. Application of Pade's approximation for the time derivative term results in two explicit and two implicit spatial differential equations. To increase predicted accuracy, the nodally exact CDR scheme for the constant-coefficient inhomogeneous convection-diffusion-reaction equation was applied in a domain of one dimension. Also, all the spatial derivatives in the source term were approximated to yield fourth-order spatial accuracy. To fully assess the proposed fourth-order-accurate temporal and spatial schemes, problems which are all amenable to exact solutions were considered. The computed L_2-error norms

Table 5. Comparison of simulated solutions obtained at $\Delta t = 10^{-1}$, 10^{-2}, 10^{-3}, and 10^{-4} for the second problem in Section 5.2 [(·) denotes CPU time]

Δt	Present Eq. (4.1)	AB Eq. (2.30)	Gear (open) Eq. (2.31)	RK Eq. (2.29)	AM Eqs. (2.21)–(2.22)	Gear (closed) Eqs. (2.23)–(2.24)	RKF Eq. (2.25)
10^{-1}	3.368E-01	4.206E+00	4.551E+00	2.325E+02	2.257E+01	3.212E+01	2.312E+00
	(2.312)	(1.687)	(1.453)	(1.437)	(1.871)	(1.593)	(2.461)
10^{-2}	2.356E-02	2.332E-01	2.785E-01	2.980E-02	1.210E-01	1.360E-01	2.563E-02
	(16.718)	(9.562)	(7.890)	(8.984)	(10.250)	(8.312)	(18.146)
10^{-3}	2.167E-03	2.712E-03	6.749E-02	2.689E-03	2.681E-03	1.287E-02	2.631E-03
	(162.312)	(87.171)	(76.781)	(86.359)	(91.375)	(86.187)	(192.698)
10^{-4}	3.372E-04	6.692E-04	2.597E-03	6.684E-04	6.686E-04	3.274E-04	5.186E-04
	(2225.453)	(886.562)	(1238.718)	(1195.671)	(1452.515)	(1354.906)	(2647.146)

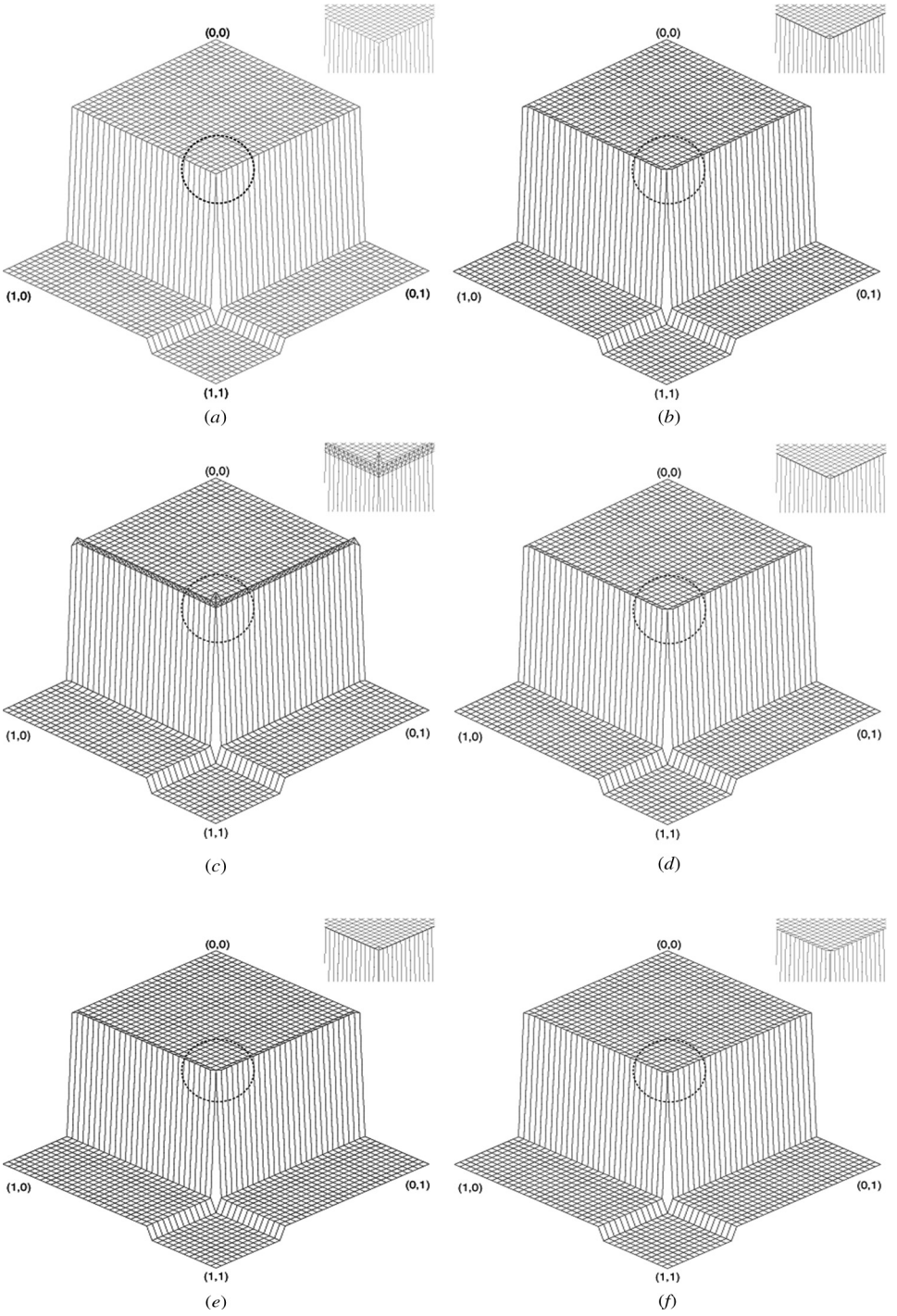

Figure 9. Simulated solution profiles for ϕ at $t = 0.6$ for the two-dimensional equation considered in Section 5.2: (*a*) present; (*b*) Adams-Bashforth (AB); (*c*) Gear (open-type); (*d*) Runge-Kutta (RK); (*e*) Adams-Moulton (AM); (*f*) Gear (closed-type).

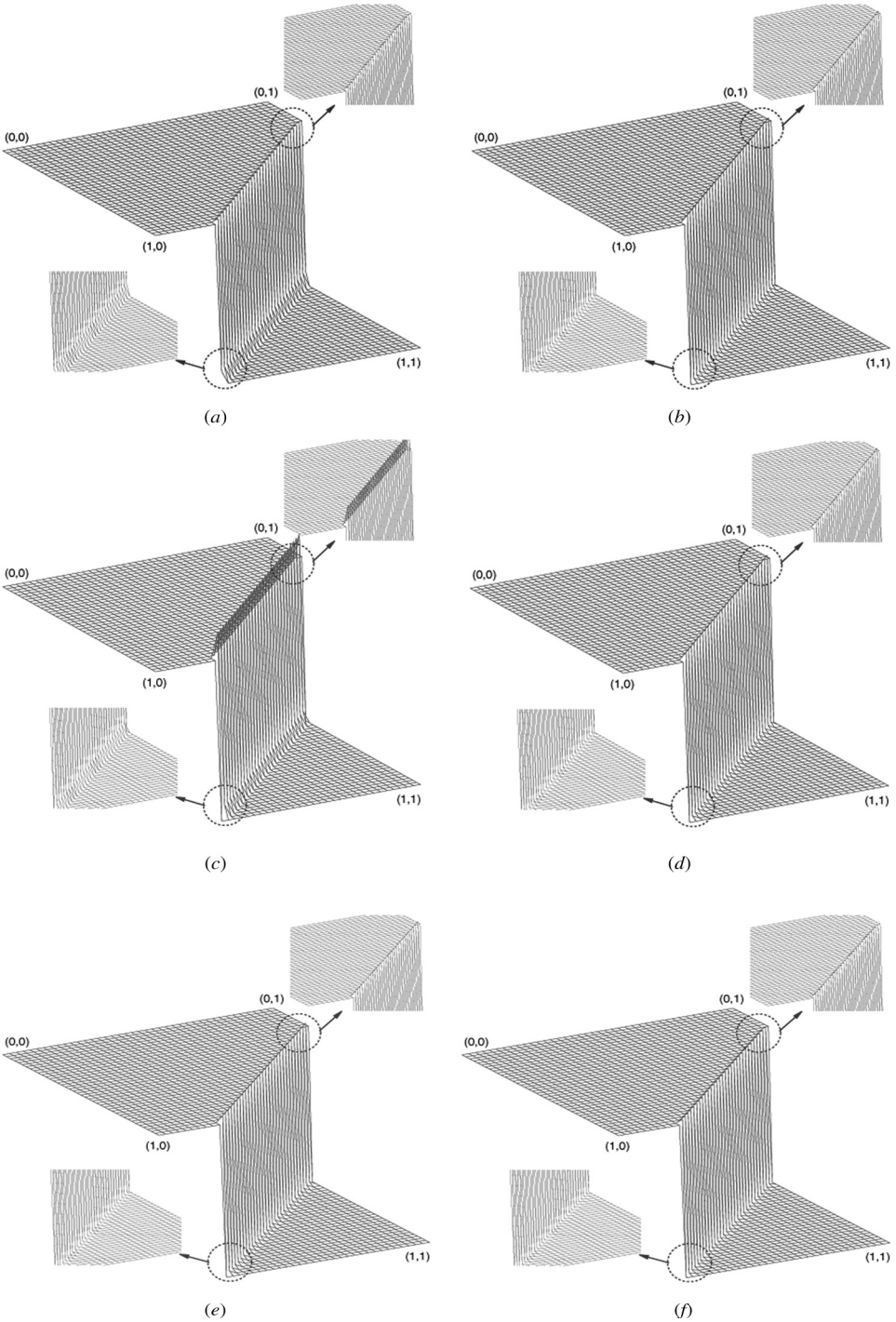

Figure 10. Simulated solution profiles at $t = 1.25$ for the two-dimensional equation considered in Section 5.2: (*a*) present; (*b*) Adams-Bashforth (AB); (*c*) Gear (open-type); (*d*) Runge-Kutta (RK); (*e*) Adams-Moulton (AM); (*f*) Gear (closed-type).

Table 6. Comparison of simulated solutions obtained at $\Delta t = 10^{-1}$, 10^{-2}, 10^{-3}, and 10^{-4} for the third problem in Section 5.2 [(·) denotes CPU time]

Δt	Present Eq. (4.1)	AB Eq. (2.30)	Gear (open) Eq. (2.31)	RK Eq. (2.29)	AM Eqs. (2.21)–(2.22)	Gear (closed) Eqs. (2.23)–(2.24)	RKF Eq. (2.25)
10^{-1}	5.951E-01	6.072E + 00	6.214E + 00	2.026E + 02	5.893E + 01	7.858E + 01	6.538E + 00
	(1.125)	(1.078)	(0.859)	(0.875)	(1.213)	(0.875)	(1.456)
10^{-2}	3.709E-02	4.451E-01	4.022E-01	1.005E-01	5.902E-01	5.487E-01	4.967E-02
	(6.140)	(4.375)	(3.609)	(4.218)	(4.500)	(3.984)	(6.978)
10^{-3}	2.304E-03	2.672E-02	4.679E-02	2.590E-03	2.611E-02	2.576E-02	2.472E-03
	(62.265)	(41.156)	(35.765)	(41.593)	(43.343)	(38.843)	(68.136)
10^{-4}	2.371E-04	1.353E-03	4.470E-03	2.352E-04	1.352E-03	4.460E-03	2.965E-04
	(654.031)	(410.156)	(340.109)	(405.140)	(423.703)	(375.687)	(679.146)

and the simulated theoretical rates of convergence demonstrate the advantage of applying the proposed convection-diffusion scheme. For the sake of completeness, theoretical studies of the proposed scheme and assessment versus other temporal schemes have also been conducted.

REFERENCES

1. Yu. I. Shokin, *The Method of Differential Approximation*, Springer-Verlag, Berlin, 1983.
2. M. Machura and R. A. Sweet, A Survey of Software for Partial Differential Equations, *ACM Trans. Math. Softw.*, vol. 6, no. 4, pp. 461–488, 1980.
3. M. Berzins, Global Error Estimation in the Method of Lines for Parabilic Equations, *SIAM J. Sci. Comput.*, vol. 9, no. 4, pp. 687–703, 1988.
4. J. Lawson, M. Berzins, and P. M. Dew, Balancing Space and Time Errors in the Method of Lines for Parabolic Equations, *SIAM J. Sci. Comput.*, vol. 12, no. 3, pp. 573–594, 1991.
5. P. Saucez, A. Vande Wouwer, and W. E. Schiesser, An Adaptive Method of Lines Solution of the Korteweg-de Vries Equation, *Comput. Math. Appl.*, vol. 35, no. 12, pp. 13–25, 1998.
6. M. Berzins, Temporal Error Control in the Method of Lines for Convection Dominated Equations, *SIAM J. Sci. Comput.*, vol. 16, no. 3, pp. 558–580, 1995.
7. W. E. Schiesser, *The Numerical Method of Lines; Integration of Partial Differential Equations*, Academic Press, San Diego, CA, 1991.
8. S. V. Pennington and M. Berzins, New NAG Library Software for First-Order Partial Differential Equations, *ACM Trans. Math. Softw.*, vol. 20, no. 1, pp. 63–99, 1994.
9. M. Berzins, P. M. Dew, and R. M. Furzeland, Developing Software for Time-Dependent Problems Using the Method of Lines and Differential Algebraic Integrators, *Appl. Numer. Math.*, vol. 5, pp. 375–397, 1989.
10. M. Berzins, Developments in the NAG Library Software for Parabolic Equations, in J. C. Mason and M. G. Cox (eds.), *Scientific Software Systems*, pp. 59–72, Chapman & Hall, 1989.
11. M. Friedman and A. Kandel, *Fundamentals of Computer Numerical Analysis*, CRC Press, Boca Raton, FL, 1994.
12. J. D. Lambert, *Computational Methods in Ordinary Differential Equations*, Wiley, Chichester, UK, 1973.
13. R. K. Lin and T. W. H. Sheu, A Four-Step Time Splitting Scheme for Convection-Diffusion Equation, *Numer. Heat Transfer B*, vol. 45, pp. 263–281, 2004.
14. G. Engeln-Müllges and F. Uhlig, *Numerical Algorithms with Fortran*, Springer-Verlag, Berlin, 1996.
15. E. Fehlbery, New High-Order Runge-Kutta Formulas with an Arbitrarily Small Truncation Error, *Z. Angew. Math. Mech.*, vol. 46, pp. 1–16, 1996.
16. M. A. Celia and W. G. Gray, *Numerical Methods for Differential Equations*, Fundamental Concepts for Scientific and Engineering Applications, Prentice-Hall, Singapore, 1992.
17. T. W. H. Sheu, C. F. Chen, W. S. Huang, and L. W. Hsieh, A Novel Two-Dimensional Convection-Diffusion Finite-Difference Scheme, *Numer. Heat Transfer B*, vol. 38, pp. 369–387, 2000.
18. Y. H. Chen and T. W. H. Sheu, Two-Dimensional Scheme for Convection-Diffusion with Linear Production, *Numer. Heat Transfer B*, vol. 37, pp. 365–377, 2000.
19. M. J. Ni, W. O. Tao, and S. J. Wang, Stability Analysis for Discretized Steady Convection-Diffusion Equation, *Numer. Heat Transfer B*, vol. 35, pp. 369–388, 1999.
20. V. Kriventsev and H. Ninokata, Effective, Locally Exact Finite-Difference Scheme for Convection-Diffusion Problems, *Numer. Heat Transfer B*, vol. 36, pp. 183–205, 1999.

21. G. A. Baker, Jr., The Theory and Application of the Pade Approximant Method, in K. A. Brueckner (ed.), *Advances in Theoretical Physics*, Vol. 1, pp. 1–58, Academic Press, New York, 1965.
22. G. A. Baker, Jr., *Essentials of Padé Approximants in Theoretical Physics*, pp. 27–38, Academic Press, New York, 1975.
23. G. A. Baker, Jr., and P. Graves-Morris, *Padé Approximants*, Cambridge University Press, New York, 1996.
24. R. P. Brent, F. G. Gustavson, and D. Y. Y Yun, Fast Solution of Toeplitz Systems of Equations and Computation of Padé Approximants, *J. Algorithms*, vol. 1, pp. 259–295, 1980.
25. D. W. Peaceman and H. H. Rachford, The Numerical Solution of Parabolic and Elliptic Differential Equations, *J. Soc. Ind. Appl. Math.*, vol. 3, pp. 28–41, 1955.
26. Y. Li, Wavenumber-Extended High-Order Upwind-Biased Finite Difference Schemes for Convective Scalar Transport, *J. Comput. Phys.*, vol. 133, pp. 235–255, 1997.
27. R. K. Lin, Development of a Numerical Method for Analyzing the Incompressible Thermal/Magnetic Fluid Flows, Ph.D. thesis, National Taiwan University, Taipei, Taiwan, 2005.
28. J. J. H. Miller, E. O'Riordan, G. I. Shishkin, and S. Wang, A Parameter-Uniform Schwarz Method for a Singularly Perturbed Reaction-Diffusion Problem with an Interior Layer, *Appl. Numer. Math.*, vol. 35, pp. 323–337, 2000.
29. J. D. Cole, On a Quasilinear Equation Occurring in Aerodynamics, *Q. Appl. Math.*, vol. 9, pp. 225–236, 1951.
30. M. Berzins and J. M. Ware, Positive Cell-Centered Finite Volume Discretization Methods for Hyperbolic Equations on Irregular Meshes, *Appl. Numer. Math.*, vol. 16, pp. 417–438, 1995.